Applied Physics Letters ARTICLE pubs.aip.org/aip/apl

# Terahertz unipolar polarimetry by second-harmonic generation in air

Cite as: Appl. Phys. Lett. **123**, 071101 (2023); doi: 10.1063/5.0162035
Submitted: 13 June 2023 · Accepted: 1 August 2023 ·
Published Online: 14 August 2023

View Online Export Citation CrossMark

Sen Mou,[1] Andrea Rubano,[2,3] Qiucheng Yu,[2] and Domenico Paparo[2,3,a)]

## AFFILIATIONS

[1]Institut de Ciencies Fotoniques, The Barcelona Institute of Science and Technology, Castelldefels, Barcelona, Spain
[2]Dipartimento di Fisica "Ettore Pancini," Università di Napoli "Federico II," Complesso Universitario di Monte Sant'Angelo, via Cintia, Napoli 80126, Italy
[3]ISASI—Institute of Applied Sciences and Intelligent Systems, Consiglio Nazionale delle Ricerche, via Campi Flegrei 34, Pozzuoli 80078, Italy

[a)]**Author to whom correspondence should be addressed:** domenico.paparo@cnr.it

## ABSTRACT

Femtosecond laser-based terahertz (THz) sources have gained attention for their potential in various applications. As for any electromagnetic radiation, the wave polarization is a critical parameter, which needs to be under control in a wide class of those applications. However, characterizing the polarization of broadband THz pulses remains challenging due to their limited efficient optics. THz air-biased coherent detection has emerged as a promising candidate. The technique employed is heterodyne detection, utilizing second-harmonic generation induced by THz radiation in laser-induced air plasmas. This approach provides exceptional spectral bandwidth and an unbounded power detection limit, rendering it highly suitable for ultra-broadband and high-power THz sources. It enables a very efficient polarization measurement too. However, recent findings have revealed that the laser-induced air plasma generated in this technique can exhibit birefringence, which in turn adds systematic errors to the polarization-state determination. In this Letter, we propose a simplified approach that utilizes a weak probe beam and avoids high-voltage DC bias-fields. Unlike the terahertz (THz) air-biased coherent detection scheme, our approach yields a unipolar, intensity-proportional signal for second-harmonic generation. The experimental results reported in this Letter show the absence of induced birefringence in air and, hence, demonstrate accurate measurements of the polarization state of ultra-broadband THz pulses. Therefore, our technique may provide valuable results in applications where the polarization state, and not the full electric field waveform, is required for analysis or characterization. Finally, we discuss a possible application of our method to the emergent field of THz singular optics.

*Published under an exclusive license by AIP Publishing.* https://doi.org/10.1063/5.0162035

23 August 2023 17:01:45

THz has garnered significant interest following the development of femtosecond laser-based THz sources, enabling the availability of table-top THz sources for numerous scientific and technological applications.[1,2] Among various methods of THz generation, considerable attention has been given to the generation via two-color mixing in plasma, primarily due to the high intensity and broadband spectrum of THz radiation emitted from this plasma.[3–6] One notable advantage of this technique is the ability to employ the full power of an intense pump laser, without encountering a thermal damage threshold.[7,8]

However, the utilization of broadband pulses in such scenarios presents several challenges, particularly when comprehensive characterization of the optical properties, such as the polarization, of these pulses is required. This difficulty arises from the scarcity of efficient and truly broadband optics in the THz range. Conversely, numerous applications necessitate the precise measurement of the polarization state of these broadband THz pulses.[9–12]

The conventional method for measuring the polarization of THz waves involves the use of solid-state detectors such as electro-optical crystals and photoconductive antennas. In this approach, the time-resolved polarization is reconstructed by measuring THz waveforms along two orthogonal directions while rotating wire-grid polarizers or polarization-sensitive detectors. However, this technique has limitations in terms of the detection bandwidth and maximum intensity, which makes it incompatible with ultra-broadband and high-power THz sources.

To address these limitations, THz air-biased coherent detection (ABCD) emerges as a promising detection technique for these novel THz sources. ABCD offers superior bandwidth and frequency resolution, making it well-suited for ultra-broadband and high-power THz


Published under an exclusive license by AIP Publishing

sources.[13,14] This technique provides, in addition, the capability for efficient polarization measurement.

ABCD operates as a heterodyne detection technique based on a third-order nonlinear process.[13] It utilizes a modulated DC bias electric field at the focal points of the fundamental wave (FW) to induce a second-harmonic signal, which serves as the local oscillator for coherent detection of the second-harmonic signal induced by the THz field. To optimize the dynamic range of the THz ABCD system, it is customary to generate a weak plasma by employing intense probe beams.

The fundamental mechanism of ABCD is elucidated through the theory of four-wave mixing. The intensity of the detected second-harmonic (SH) signal can be expressed using the following formula:

$$I_{2\omega} \propto \left(E_{2\omega}^{THz} + E_{2\omega}^{DC}\right)^2 \propto \left(\chi^{(3)} I_\omega\right)^2 I^{THz} + \left(\chi^{(3)} I_\omega\right)^2 |E^{DC}|^2 + \left(\chi^{(3)} I_\omega\right)^2 E^{THz} E^{DC}. \quad (1)$$

In this equation, $E_{2\omega}^{THz}$ represents the SH induced by the THz electric-field, $E^{THz}$, while $E_{2\omega}^{DC}$ represents the SH optical field induced by the electric-field amplitude of the DC bias, $E^{DC}$. Additionally, $I_\omega$ is the intensity of the FW, and $\chi^{(3)}$ is the third-order susceptibility driving the four-wave mixing process. $I^{THz}$ denotes the intensity of the THz wave, which contributes to the "unipolar" first term in Eq. (1). This term does not carry information about the phase of the THz wave and is canceled out by the heterodyne process when using the ABCD method. By measuring $I_{2\omega}$ with positive and negative DC bias and taking the difference between the two measurements, it is possible to cancel the first two terms and, thus, single out the last term in Eq. (1). This allows for the extraction of the THz waveform.

By measuring the latter waveform along two orthogonal directions, any elliptical polarization of the THz pulse may be obtained. Based on Eq. (1), this reconstruction can be achieved simply by rotating the detector, which corresponds to rotating the orientations of the fundamental wave (FW) and DC bias along two orthogonal directions. Recently, a study introduced a technique that utilizes a quad-electrode ABCD system to detect THz waves with arbitrary polarization, enabling the simultaneous acquisition of the THz orthogonal component.[15]

However, recent findings have demonstrated that under these circumstances, the plasma can exhibit birefringence, causing a modification in the polarization state of the FW used as the probe beam.[16] Consequently, the measurement of the THz wave's polarization state is affected by systematic errors, particularly when the polarization of the FW closely aligns with the analyzer direction and is orthogonal to the polarization of the THz wave.

In this Letter, we propose a simplified scheme that exploits the first term of Eq. (1), i.e., the unipolar component, and avoids, hence, the use of intense probe-beams and high-voltage DC bias-fields. Therefore, we name our technique terahertz unipolar polarimetry (TUP). Our demonstration establishes that there is no deviation from the theoretical prediction at any angle of the fundamental wave, in contrast to the observations made by Zhang *et al.*[16] This observation highlights the complete absence of induced birefringence effects in the air that could potentially compromise the accurate reconstruction of the THz wave polarization in our method.

We wish to highlight a crucial element of our proposed technique: although our method does not enable the tracking of transverse electric-field components throughout the pulse duration, as accomplished by the ABCD method, it does allow the detection of any arbitrary polarization state of a THz pulse. This particular information suffices for applications like THz dichroism experiments.[9] In such scenarios, our approach can provide precise results without the need for high-voltage DC bias-fields or introducing systematic errors that arise from induced birefringence effects.

It should be noted that $\chi^{(3)}$ is not a simple constant, but rather a four-index tensor with 21 nonzero elements, denoted as $\chi_{ijlm}$. This adds complexity to Eq. (1) for the SH optical field, which appears in the absence of a DC bias-field,

$$E_i^{2\omega} \propto \chi_{ijlm} E_j^{THz} E_l^{\omega} E_m^{\omega}, \quad (2)$$

where $E_l^{\omega}$ is the FW field. In the latter equation, the Einstein rule on repeated indices is applied.

The third-order susceptibility of an isotropic media, such as air, has only three independent elements, as shown in Table I. We assume that these elements are real, i.e., the frequency of both the FW and its second-harmonic is far from resonances. Furthermore, these elements satisfy the following equation:[17]

$$\chi_4 \equiv \chi_{xxxx} = \chi_{yyyy} = \chi_{zzzz} = \chi_{xxyy} + \chi_{yxyx} + \chi_{yxxy}. \quad (3)$$

Since air is an isotropic medium, we can choose the reference system arbitrary. In Fig. 1, we set the $\hat{z}$ axis parallel to the beam propagation and the $\hat{x}$ axis parallel to the axis of the polarizer used to analyze the polarization state of the second-harmonic beam. The FW polarization forms an angle with the $\hat{x}$-axis equal to $\alpha$, while we consider a THz beam with an arbitrary linear polarization forming an angle of $\gamma$ with the $\hat{x}$-axis.

In the supplementary material, we report the details of the calculation that lead to the following expressions for the components of the generated second-harmonic field:

$$E_x^{2\omega} = A I_\omega (\chi_2 + \chi_3)\left[\chi_a \cos^2\alpha E_x^{THz} + \chi_b \sin^2\alpha E_x^{THz} + \sin\alpha\cos\alpha E_y^{THz}\right], \quad (4)$$

$$E_y^{2\omega} = A I_\omega (\chi_2 + \chi_3)\left[\chi_b \cos^2\alpha E_y^{THz} + \chi_a \sin^2\alpha E_y^{THz} + \sin\alpha\cos\alpha E_x^{THz}\right], \quad (5)$$

where $A$ is a proportionality constant common to both components; $\chi_a = \chi_4/(\chi_2 + \chi_3)$ and $\chi_b = \chi_1/(\chi_2 + \chi_3)$.

While the $x$-component can be measured directly, for analyzing the $y$-component we need to insert a half-waveplate that projects the latter on the polarizer axis. For general purposes, we assume that the optical axis of this waveplate forms an angle of $\beta/2$ with the $\hat{x}$-axis.

**TABLE I.** Form of the third-order susceptibility tensor in air. Note the new symbols $\chi_1$, $\chi_2$, and $\chi_3$ introduced to simplify notation.

| Isotropic medium: 21 elements; 3 independent |
|---|
| $\chi_1 \equiv \chi_{yyzz} = \chi_{zzyy} = \chi_{zzxx} = \chi_{xxzz} = \chi_{xxyy} = \chi_{yyxx}$ |
| $\chi_2 \equiv \chi_{yzyz} = \chi_{zyzy} = \chi_{zxzx} = \chi_{xzxz} = \chi_{xyxy} = \chi_{yxyx}$ |
| $\chi_3 \equiv \chi_{yzzy} = \chi_{zyyz} = \chi_{zxxz} = \chi_{xzzx} = \chi_{xyyx} = \chi_{yxxy}$ |

23 August 2023 17:01:45


Published under an exclusive license by AIP Publishing

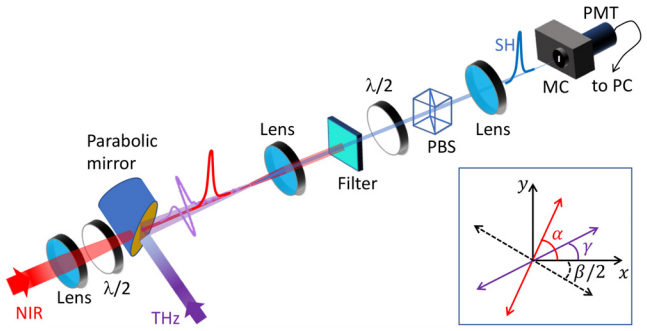


**FIG. 1.** Experimental scheme of the apparatus. FW and THz beams are collinearly focused on the same point, respectively, by a lens and a hole-drilled off-axis parabolic mirror. SH is analyzed by a combination of the half-waveplate and polarizing beam splitter (PBS) with the axis parallel to the $\hat{x}$ axis. A monochromator (MC) further rejects spurious signals, and a photomultiplier tube (PMT) measures the SH intensity. Lower right inset shows the geometry of the different polarizations and half-waveplate axis: FW (red); THz wave (purple); half-wave plate axis (dotted black).

Then the second-harmonic optical field transmitted behind the polarizer is given by

$$E_{2\omega}(\alpha,\beta) = \cos\beta E_x^{2\omega} + \sin\beta E_y^{2\omega}, \tag{6}$$

and the intensity measured by the detector is then $I_{2\omega}(\alpha,\beta) = K\left|E_{2\omega}(\alpha,\beta)\right|^2$.

As we will show in the following, the knowledge of the ratios $\chi_a$ and $\chi_b$ allows us to use Eqs. (4) and (5) to measure any arbitrary polarization of the THz pulse. The experimental determination of these ratios can be achieved with high accuracy by scanning the second-harmonic signal at a given angle $\gamma$ while varying the angles $\alpha$ and $\beta$. To this aim, we utilize the experimental setup depicted in Fig. 1. Broadband THz pulses are generated through a four-wave mixing process driven by a plasma created in air by focusing a FW beam and its SH. The FW beam is delivered by a regeneratively amplified femtosecond laser system (Coherent Legend). A small part of the FW beam is used as probe-beam for detecting the THz pulse. The laser generates pulses with a central wavelength of around 800 nm, a pulse duration of approximately 35 fs, an output power of approximately 3.7 W, and a repetition rate of 1 kHz. A more detailed description of our THz source can be found in the supplementary material of our former publication.[18] The THz beam is focused by the parabolic mirror, and its polarization is set in the $x$ direction ($\gamma = 0$) by a wire grid polarizer from TYDEX.[19] This polarizer is constructed on a polypropylene substrate, which naturally restricts the initial bandwidth of the THz pulse to the 0.15–20 THz range. The focused probe beam passes through the hole of an off-axis parabolic mirror so to propagate collinearly with the THz beam. The generated SH encounters a low-pass filter that rejects most of the fundamental probe beam. Then the SH polarization is analyzed by a combination of a half wave plate and a polarizing beam splitter (PBS). The selected component is further filtered by a monochromator and finally detected by a photomultiplier tube (PMT).

Figure 2 displays an example of the SH signal along with the measured THz pulse using the ABCD technique (black line). For the latter, a DC bias of 10 kV/cm, modulated at a frequency of 500 Hz, is

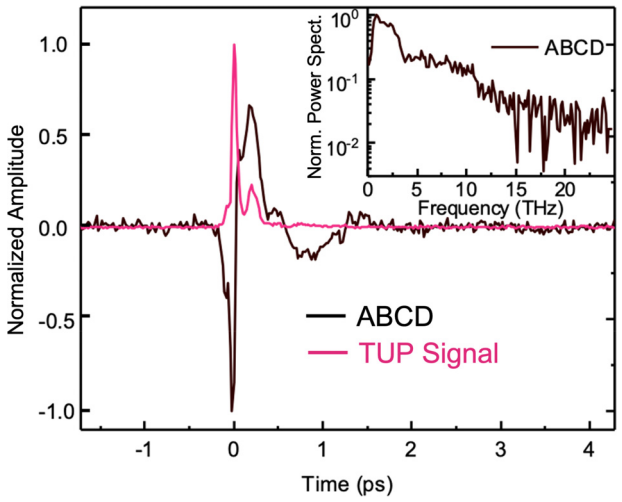


**FIG. 2.** Main panel: the THz pulse as measured by means of the ABCD technique (black curve) and the unipolar SH signal (TUP) obtained when the local oscillator provided by the bias DC field is switched off (red curve). Inset: the power spectrum of the THz pulse (FFT power spectrum of the ABCD waveform), showing that there is a significant signal up to 15 THz.

applied as a local oscillator at the focus of the probe beam. The inset of Fig. 2 showcases the power spectrum of the THz pulse. It is important to mention that the spectrum is constrained by the polarizer employed to optimize the polarization of our THz pulses and not by the generation method itself. Taking into account the pulse duration of the fundamental beam and the four-wave mixing process, the maximum extent of the THz pulse spectrum is approximately 40 THz. These values are commonly observed in experimental settings as well.[20] It is important to mention that the wire-grid polarizer serves the purpose of precise calibration of the technique but is not used during the polarization measurement. As a result, our technique possesses an almost boundless bandwidth in principle. Despite the present limitation of our experiment, it is noteworthy that the bandwidth of our pulse significantly exceeds that of the work by Zhang *et al.*[16] The red curve in Fig. 2 represents instead the unipolar SH (TUP) signal obtained by switching off the DC bias-voltage. For all subsequent measurements, the delay between the THz pulse and the probe beam is adjusted to coincide with the peak of the unipolar second-harmonic signal. We note that the signal-to-noise ratios of ABCD and TUP are different, which can be explained by means of Eq. (1). The ratio between the TUP and ABCD signals is $E^{THz}/E^{DC}$. Since $E^{THz}$ is more than ten times larger than $E^{DC}$ in the experiment, the TUP signal exhibits a better signal-to-noise ratio than the ABCD signal. Additionally, we observe that the pulse duration of the TUP signal is shorter than that of the ABCD. The strongest THz electric field, compared with the DC field, is capable of detecting broader spectrum tails, leading to a shorter signal duration. We also point out that there is a limitation in the maximum DC electric field one can apply. A DC electric field of around 30 kV/cm can ionize the air. Thus, the difference between the TUP and ABCD signals becomes more evident when the THz field higher than 100 kV/cm is measured.

First, we determine the ratios $\chi_a$ and $(\chi_4 + \chi_1)/(\chi_2 + \chi_3)$ by measuring $I_{2\omega}(\alpha, 0)$ and $I_{2\omega}(\pi/4, \beta)$. In the case $I_{2\omega}(\alpha, 0)$, only two

23 August 2023 17:01:45


Published under an exclusive license by AIP Publishing

adjustable parameters are involved: an overall scale factor and the ratio $\chi_a$. On the other hand, for the function $I_{2\omega}(\pi/4, \beta)$, the adjustable parameters consist of an overall scale factor and the ratio $(\chi_4 + \chi_1)/(\chi_2 + \chi_3)$. Detailed calculations regarding these measurements can be found in the supplementary material.

Figure 3 presents the results of these measurements along with the corresponding fits (depicted as solid lines). Remarkably, the fits exhibit excellent agreement with the experimental data. Notably, in panel (a), agreement holds true for any value of $\alpha$, thereby demonstrating a complete absence of induced birefringence in air.

The obtained values for the relevant adjustable parameters are $\chi_a = 2.53 \pm 0.08$ and $(\chi_4 + \chi_1)/(\chi_2 + \chi_3) = 2.54 \pm 0.09$. Further calculations yield $\chi_4/(\chi_2 + \chi_3) = 1.82 \pm 0.06$ and $\chi_1/(\chi_2 + \chi_3) = 0.72 \pm 0.03$. These results are consistent with Eq. (3) within the statistical errors.

Based on these results, we can fix all the adjustable fitting parameters for all the other angle combinations with the exception of an overall scale factor. The results of these analyses are reported in Fig. 4, where in panel (a), we display the measurement of $I_{2\omega}(\alpha, \beta)$ at varying $\alpha$ and $\beta$; while in panel (b), we show the results of the fitting procedure explained above. Again, we highlight an excellent agreement between experimental data and fitting curves. In Fig. S2 of the supplementary material, we provide with other exemplary polar plots extracted from Fig. 4 and analogous to those presented in Fig. 3.

Following the calibration process, we proceed to discuss the application of the outlined methodology for determining almost any arbitrary polarization of the THz pulse. Let us consider a THz pulse with an arbitrary average polarization. According to the Jones formalism, the THz optical field can be expressed as[21]

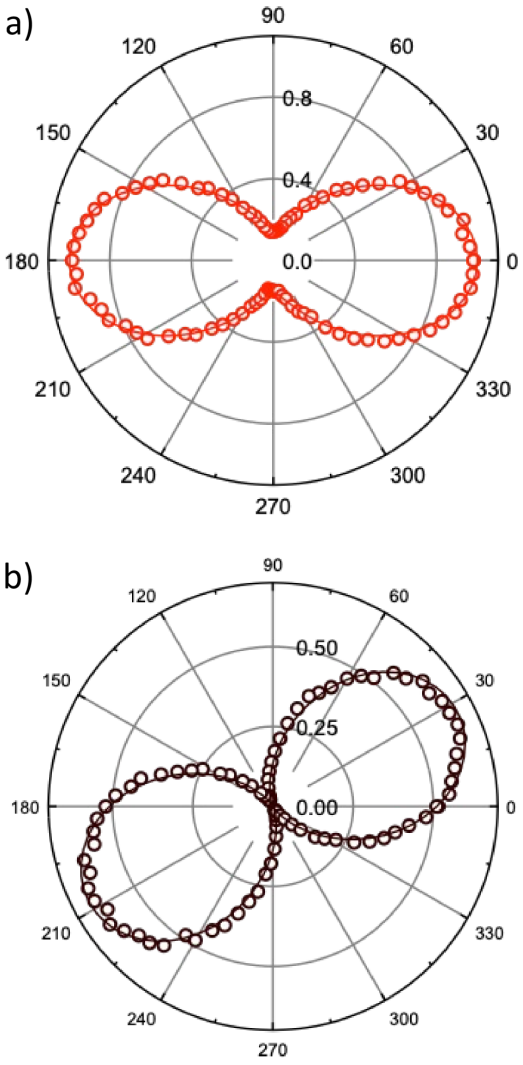


**FIG. 3.** The polar plots of $I_{2\omega}(\alpha, 0)$ and $I_{2\omega}(\pi/4, \beta)$ are reported as a function of $\alpha$ and $\beta$ in panels (a) and (b), respectively (open circles). The red and black solid lines are the corresponding fitting curves, which allow a determination of the ratios $\chi_a$ and $(\chi_4 + \chi_1)/(\chi_2 + \chi_3)$.

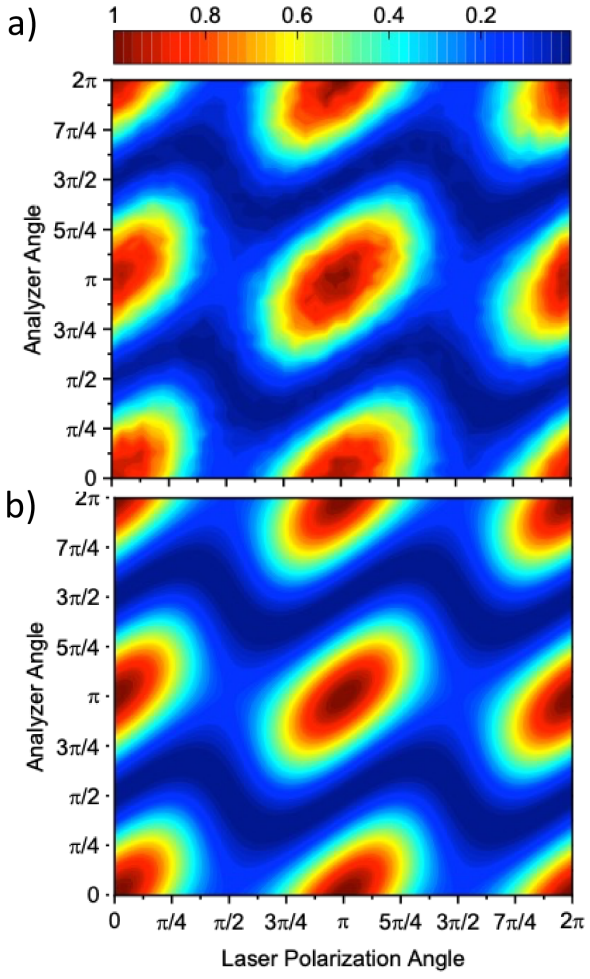


**FIG. 4.** In panel (a), the SH intensity $I_{2\omega}(\alpha, \beta)$ as a function of $\alpha$ and $\beta$ at $\gamma = 0$ is reported. In panel (b), the corresponding theoretical results as calculated by squaring Eq. (5) are displayed. The agreement is excellent for any pair of angles $\alpha$ and $\beta$.

23 August 2023 17:01:45


Published under an exclusive license by AIP Publishing

$$\begin{bmatrix} E_x^{THz} \\ E_y^{THz} \end{bmatrix} = \begin{bmatrix} a \\ b(\cos\delta + i\sin\delta) \end{bmatrix}. \quad (7)$$

By substituting Eq. (7) into Eqs. (4) and (5), we obtain the following results:

$$I_{2\omega}(\alpha,0) = KA^2 I_\omega^2 (\chi_2+\chi_3)^2 b^2 \Big[ \left(\chi_a \cos^2\alpha + \chi_b \sin^2\alpha\right)^2 r^2 + \sin^2\alpha \cos^2\alpha + 2r\cos\delta \sin\alpha\cos\alpha\left(\chi_a\cos^2\alpha + \chi_b \sin^2\alpha\right)\Big], \quad (8)$$

$$I_{2\omega}(\alpha,\pi/2) = KA^2 I_\omega^2 (\chi_2+\chi_3)^2 b^2 \Big[ \left(\chi_b \cos^2\alpha + \chi_a \sin^2\alpha\right)^2 + r^2 \sin^2\alpha \cos^2\alpha + 2r\cos\delta \sin\alpha\cos\alpha\left(\chi_b\cos^2\alpha + \chi_a \sin^2\alpha\right)\Big], \quad (9)$$

where $r = a/b$.

Figure 5 illustrates that by measuring $I_{2\omega}(\alpha,0)$ and $I_{2\omega}(\alpha,\pi/2)$ and fitting the results with Eqs. (8) and (9), it is possible to distinguish between different polarization states. It is important to note that, apart from a common scaling factor, the only fitting parameters are $r$ and $\delta$, i.e., the polarization state parameters. In panel (b), the simulations representing circular polarizations with opposite handedness, shown in panel (a), are presented. For the sake of conciseness, the focus in the figure is solely on the $I_{2\omega}(\alpha,0)$ signal. However, to avoid ambiguities in the polarization determination, it is always necessary to measure both $I_{2\omega}(\alpha,0)$ and $I_{2\omega}(\alpha,\pi/2)$, as we will emphasize later and as shown in Fig. S3 of the supplementary material. The results clearly demonstrate that our method cannot distinguish the handedness. This outcome was expected since we measured only the intensity, resulting in a loss of information regarding the handedness sign. However, in Sec. 2 of the supplementary material, we show that this information, if needed, can be recovered by measuring the phase of the SH signal by interference with a reference SH signal generated by a suitable nonlinear crystal.[22] As shown in the supplementary material, this leads only to a slight modification of the apparatus displayed in Fig. 1. Here, to keep the main message straight, we focus only on the basic TUP technique.

The other panels in Fig. 5 depict additional examples of polarizations (linear and generic elliptical) and their corresponding TUP diagrams. Based on the previous observation, our discussion primarily focuses on right-handed elliptical polarization. Panels (c) and (d) of Fig. 5 demonstrate the clear differentiation between a linear polarization and an elliptical polarization with the major axis along the $\hat{y}$-axis, as evidenced by the significantly distinct polar plots. Not shown in the figure (for more exemplary plots, we remind to the supplementary material), $I_{2\omega}(\alpha,\pi/2)$ exhibits identical polar plots for both these polarization states. Due to symmetry, the situation is reversed in the case of linear polarization and elliptical polarization with the major axis oriented along the $\hat{x}$-axis. Consequently, $I_{2\omega}(\alpha,0)$ exhibits the same graphs, while $I_{2\omega}(\alpha,\pi/2)$ behaves similarly to the graphs in panel (d). This demonstrates that in order to reconstruct the polarization state without ambiguity, it is necessary to measure both $I_{2\omega}(\alpha,0)$ and $I_{2\omega}(\alpha,\pi/2)$. Furthermore, a global fitting procedure on both signals always provides with a more accurate determination of the polarization state. This becomes particularly important when the two graphs start to closely resemble each other, as observed for linear and elliptical polarizations with symmetry axes at angles other than 0° and 90° (see Fig. S3 for an example).

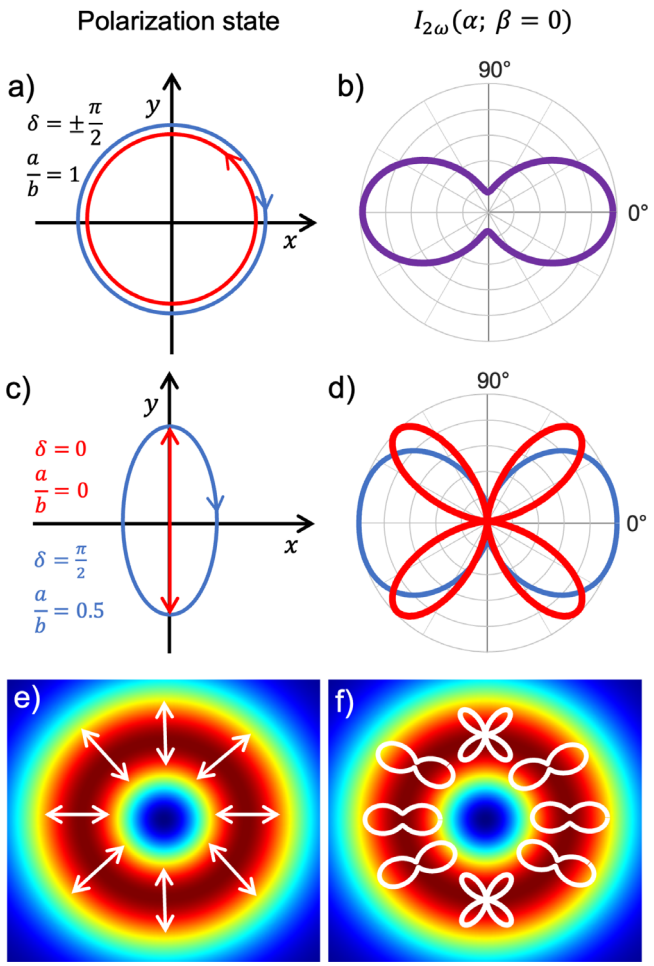


**FIG. 5.** In panel (a), the two possible circular polarizations with the corresponding values of $\delta$ and $a/b$ are reported: right-handed (blue solid line; $\delta = \pi/2$) and left-handed (red solid line; $\delta = -\pi/2$). The two circle diameters are slightly different for clarity. In panel (b), the corresponding TUP diagrams for both polarizations are reported. They are indistinguishable showing the impossibility of retrieving the polarization handedness. In panel (c), an example of linear (red lines) and elliptical (blue line) polarizations is shown. In panel (d), the corresponding TUP diagrams are drawn. In panel (e), we display an example of the vector beam with a radial distribution of linear polarization. The TUP pattern that is obtained in this case is shown in panel (f).

Finally, in panels (e) and (f), we present a demonstration of the application of TUP for measuring the polarization distribution of THz vector beams. These beams exhibit varying spatial polarization and intensity distributions, and their significance in future THz photonic devices and applications is expected to increase over time, mirroring the trend observed in the visible range.[23,24] To measure these characteristics by means of TUP, a straightforward approach involves scanning the focus of the probe beam across the transverse plane of the THz beam, where the size of the THz beam in the focus is significantly

23 August 2023 17:01:45


Published under an exclusive license by AIP Publishing

larger than the probe beam's waist. Figure 5(e) illustrates a vector beam with a radial distribution of linear polarization, while Fig. 5(f) presents the corresponding TUP diagram.

In the context of measuring vector beams, our method offers notable benefits owing to its simplicity and speed. By avoiding the need for complete waveform reconstruction, we achieve lower time-resolution and hence shorter measurement durations. This becomes especially crucial when working with polarization maps containing numerous points, as time-efficiency becomes a critical consideration.

In this Letter, we have demonstrated a straightforward method for measuring the arbitrary polarization state of broadband and high-energy THz pulses. Our method offers several advantages. We utilize low-intensity probe beams, ensuring measurements free from systematic errors caused by induced birefringence in air. Additionally, we eliminate the need for applying DC bias voltages, which often complicate experiments in non-trivial ways. In principle, our method can detect the full bandwidth of the input pulse, and it is much more efficient in terms of measurement time. We believe that the TUP technique is a valid alternative to present options and the unique choice when dealing with broadband and high-energy THz pulses.

See the supplementary material for a detailed theoretical derivation to support all the equations reported in the main article. Moreover, we provide with additional examples of polar plots, as the ones reported in Fig. 3, for different values of the angles $\alpha$ and $\beta$. We also display additional examples of polar plots for different polarization states, as the ones reported in Fig. 5. Finally, we describe a possible improvement of our technique to recover the capability of determining the polarization handendness.

The research leading to these results has received funding from European Union under Grant Agreement No. 101046651.

## AUTHOR DECLARATIONS

### Conflict of Interest

The authors have no conflicts to disclose.

### Author Contributions

**Sen Mou:** Data curation (lead); Investigation (lead); Software (equal); Writing – review & editing (equal). **Andrea Rubano:** Conceptualization (equal); Methodology (equal); Software (lead); Supervision (equal); Writing – review & editing (equal). **Qiucheng Yu:** Investigation (equal). **Domenico Paparo:** Conceptualization (lead); Formal analysis (lead); Funding acquisition (lead); Methodology (equal); Project administration (lead); Resources (lead); Supervision (equal); Writing – original draft (lead); Writing – review & editing (equal).

## DATA AVAILABILITY

The data that support the findings of this study are available from the corresponding author upon reasonable request.

## REFERENCES

[1]S. S. Dhillon, M. S. Vitiello, E. H. Linfield, A. G. Davies, M. C. Hoffmann, J. Booske, C. Paoloni, M. Gensch, P. Weightman, G. P. Williams, E. Castro-Camus, D. R. S. Cumming, F. Simoens, I. Escorcia-Carranza, J. Grant, S. Lucyszyn, M. Kuwata-Gonokami, K. Konishi, M. Koch, C. A. Schmuttenmaer, T. L. Cocker, R. Huber, A. G. Markelz, Z. D. Taylor, V. P. Wallace, J. A. Zeitler, J. Sibik, T. M. Korter, B. Ellison, S. Rea, P. Goldsmith, K. B. Cooper, R. Appleby, D. Pardo, P. G. Huggard, V. Krozer, H. Shams, M. Fice, C. Renaud, A. Seeds, A. Stoehr, M. Naftaly, N. Ridler, R. Clarke, J. E. Cunningham, and M. B. Johnston, "The 2017 terahertz science and technology roadmap," J. Phys. D: Appl. Phys. **50**, 043001 (2017).
[2]Y.-S. Lee, *Principles of Terahertz Science and Technology* (Springer, New York, 2009).
[3]D. J. Cook and R. M. Hochstrasser, "Intense terahertz pulses by four-wave rectification in air," Opt. Lett. **25**(16), 1210–1212 (2000).
[4]T. Bartel, P. Gaal, K. Reimann, M. Woerner, and T. Elsaesser, "Generation of single-cycle THz transients with high electric-field amplitudes," Opt. Lett. **30**(20), 2805–2807 (2005).
[5]X. Xie, J. Dai, and X. C. Zhang, "Coherent control of THz wave generation in ambient air," Phys. Rev. Lett. **96**(7), 075005 (2006).
[6]A. Rubano, S. Mou, L. Marrucci, and D. Paparo, "Terahertz hyper-Raman time-domain spectroscopy," ACS Photonics **6**(6), 1515–1523 (2019).
[7]K. Y. Kim, A. J. Taylor, J. H. Glownia, and G. Rodriguez, "Coherent control of terahertz supercontinuum generation in ultrafast laser–gas interactions," Nat. Photonics **2**(10), 605–609 (2008).
[8]V. A. Andreeva, O. G. Kosareva, N. A. Panov, D. E. Shipilo, P. M. Solyankin, M. N. Esaulkov, P. González de Alaiza Martínez, A. P. Shkurinov, V. Makarov, L. Bergé, and S. L. Chin, "Ultrabroad terahertz spectrum generation from an air-based filament plasma," Phys. Rev. Lett. **116**(6), 063902 (2016).
[9]W. J. Choi, S. Cheng, T. B. Huang, S. Zhang, T. B. Norris, and N. A. Kotov, "Terahertz circular dichroism spectroscopy of biomaterials enabled by kirigami polarization modulators," Nat. Mater. **18**, 820–826 (2019).
[10]S. Zhang, J. Zhou, Y. S. Park, J. Rho, R. Singh, S. Nam, A. K. Azad, H. T. Chen, X. Yin, A. J. Taylor, and X. Zhang, "Photoinduced handedness switching in terahertz chiral metamolecules," Nat. Commun. **3**, 942 (2012).
[11]S. Bordacs, I. Kezsmarki, D. Szaller, L. Demko, N. Kida, H. Murakawa, Y. Onose, R. Shimano, T. Room, U. Nagel, S. Miyahara, N. Furukawa, and Y. Tokura, "Chirality of matter shows up via spin excitations," Nat. Phys. **8**, 734 (2012).
[12]I. Crassee, M. Orlita, M. Potemski, A. L. Walter, M. Ostler, T. Seyller, I. Gaponenko, J. Chen, and A. B. Kuzmenko, "Intrinsic terahertz plasmons and magnetoplasmons in large scale monolayer graphene," Nano Lett. **12**, 2470 (2012).
[13]N. Karpowicz, J. Dai, X. Lu, Y. Chen, M. Yamaguchi, H. Zhao, X. C. Zhang, L. Zhang, C. Zhang, M. Price-Gallagher, C. Fletcher, O. Mamer, A. Lesimple, and K. Johnson, "Coherent heterodyne time-domain spectrometry covering the entire 'terahertz gap'," Appl. Phys. Lett. **92**, 011131 (2008).
[14]I. C. Ho, X. Y. Guo, and X. C. Zhang, "Design and performance of reflective terahertz air-biased-coherent-detection for time-domain spectroscopy," Opt. Express **18**, 2872 (2010).
[15]Z. H. Lu, D. W. Zhang, C. Meng, L. Sun, Z. Y. Zhou, Z. X. Zhao, and J. M. Yuan, "Polarization-sensitive air-biased-coherent-detection for terahertz wave," Appl. Phys. Lett. **101**, 081119 (2012).
[16]J. Zhang, "Polarization-dependent study of THz air-biased coherent detection," Opt. Lett. **39**, 4096–4099 (2014).
[17]R. W. Boyd, *Nonlinear Optics* (Elsevier, Oxford, 2008).
[18]S. Mou, A. Rubano, and D. Paparo, "Broadband terahertz spectroscopy of imidazolium-based ionic liquids," J. Phys. Chem. B **122**(12), 3133–3140 (2018).
[19]See https://www.tydexoptics.com/products/thz_polarizers/thz_polarizers1/ for the transmission spectra of the wire-grid polarizer.
[20]M. D. Thomson, V. Blank, and H. G. Roskos, "Terahertz white-light pulses from an air plasma photo-induced by incommensurate two-color optical fields," Opt. Express **18**(22), 23173–23182 (2010).
[21]B. E. A. Saleh and M. C. Teich, *Fundamentals of Photonics* (John Wiley & Sons, Inc., 2019).
[22]A. Savoia, D. Paparo, P. Perna, Z. Ristic, M. Salluzzo, F. M. Granozio, U. S. di Uccio, C. Richter, S. Thiel, J. Mannhart, and L. Marrucci, "Polar catastrophe and electronic reconstructions at the $LaAlO_3/SrTiO_3$ interface:

23 August 2023 17:01:45


Published under an exclusive license by AIP Publishing

Evidence from optical second harmonic generation," Phys. Rev. B **80**, 075110 (2009).
[23]J. J. J. Nivas, E. Allahyari, F. Cardano, A. Rubano, R. Fittipaldi, A. Vecchione, D. Paparo, L. Marrucci, R. Bruzzese, and S. Amoruso, "Surface structures with unconventional patterns and shapes generated by femtosecond structured light fields," Sci. Rep. **8**, 13613 (2018).
[24]B. Piccirillo, D. Paparo, A. Rubano, A. Andreone, M. Rossetti Conti, D. Giove, V. Vicuña-Hernández, C. Koral, M. R. Masullo, G. Mettivier, M. Opromolla, G. Papari, A. Passarelli, G. Pesce, V. Petrillo, E. Piedipalumbo, M. Ruijter, P. Russo, and L. Serafini, "Liquid crystal-based geometric phase-enhanced platform for polarization and wavefront analysis techniques with the short-terahertz FEL oscillator TerRa@ BriXSinO," Symmetry **15**, 103 (2022).

23 August 2023 17:01:45


Published under an exclusive license by AIP Publishing